Influence of the repulsive Coulomb barrier on photoelectron spectra and angular distributions in a resonantly excited dianion.

Daniel A. Horke[1][†]*, Adam S. Chatterley*[1,2] *and Jan R. R. Verlet*[1]*

[1]Department of Chemistry, University of Durham, Durham DH1 3LE, United Kingdom

[2]Department of Chemistry, University of Warwick, Coventry CV4 7AL, United Kingdom

* Corresponding author: j.r.r.verlet@durham.ac.uk

[†] Current address: Centre for Free-Electron Laser Science, DESY, Notkestr. 85, 22607 Hamburg, Germany

ABSTRACT

A photoelectron imaging study of the gas-phase dianion of pyrromethene-556 is presented. The photoelectron spectra and angular distributions following resonant excitation of the S_1 excited state with nanosecond and femtosecond laser pulses are compared, and the influence of the repulsive Coulomb barrier (RCB) in both cases evaluated. Photoelectron angular distributions show the effect of molecular alignment due to an allowed electronic excitation and can be understood qualitatively based on the calculated RCB surface using the Local Static Approximation. Comparison between femtosecond and nanosecond excitation reveals marked differences in the photoelectron spectra. While femtosecond experiments confirm that tunneling through the RCB is adiabatic, nanosecond experiments show a broad photoelectron feature peaking near the RCB maximum. This is explained in terms of the lifetime of internal conversion, which has been determined by time-resolved photoelectron spectroscopy to be ~120 ps: as this is faster than the nanosecond laser pulses, multiple photons can be absorbed through the $S_1 \leftarrow S_0$ transition which leads to large amounts of internal energy and enables electron detachment directly above the RCB. Fragmentation and detachment from the monoanion is also inferred by the presence of photoelectrons emitted at very low kinetic energy. Our results highlight the difficulty in interpreting photoelectron spectra of polyanions in which a resonant state is excited.

2

I. INTRODUCTION

Gas-phase molecular polyanions (also commonly referred to as multiply-charged anions or multianions) have received considerable scientific attention in recent years. [1-3] This is partly due to the ubiquity of these systems in the condensed phase and in nature, but also due to their unusual electronic properties when isolated. While the presence of multiple repelling charges induces an inherent instability in an isolated polyanion, there is also an inherent electronic stability present. [1, 4-10] This arises from the balance of Coulomb repulsion between the excess negative charges and the attraction between the charges and the molecular nuclei. The result is the formation of a repulsive Coulomb barrier (RCB) to electron detachment. [10-14] The presence of the RCB has led to the observation of phenomena such as polyanions with negative binding energy[9, 15] and low-energy cutoffs in photoelectron (PE) spectra, below which no electrons can be emitted directly. [16]

The exact shape and height of the RCB is strongly dependent on the location of excess charges within the molecular skeleton and can strongly affect the direction of detached photoelectrons. Photoelectron angular distributions (PADs) measured in PE imaging experiments can therefore be used as a probe for the shape of the RCB, [17-20] while the PE spectrum yields information about the RCB height. [8]

Time-resolved studies of the RCB have only recently been reported, in which electron tunneling through the barrier has been observed to occur on characteristic time-scales of a few to 100s of picoseconds. [5, 21-23] Recently, our group has shown that this tunneling process is strongly adiabatic, conserving internal energy during the tunneling event. [21] Hence, the electron tunneling can be viewed as a diagonal transition and consequently the usual correlation between the electron binding energy (*eBE*) and electron kinetic energy (*eKE*), *eBE* = *hv* − *eKE*, is not necessarily valid.

This was shown to be the case for the doubly-deprotonated fluorescein dianion, [21] but is probably quite general and has very recently also been observed in other systems. [17, 22, 23] The current study aims to provide more detailed insight into this behavior and how the PE spectra and PADs produced following resonant tunneling are sensitive to the pulse duration of the excitation laser field.
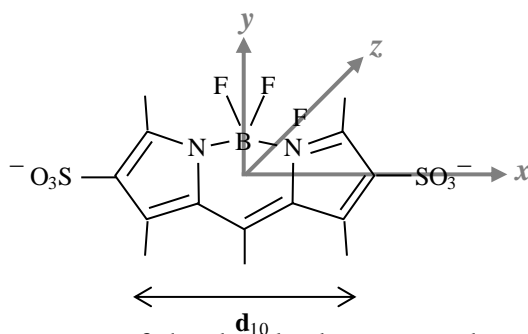

Figure 1: Molecular structure of the doubly deprotonated pyrromethene-556 dianion (PM^{2-}) with the Cartesian reference frame defined. Also shown is the direction of the transition dipole moment, $\mathbf{d}_{10}$, for excitation from S_0 to S_1.

PADs in polyanions are potentially very informative because the anisotropy of the RCB, which is determined by the location of the excess charges, can influence the trajectories of the outgoing PE. We have recently demonstrated that such information can be attained from an aligned sample created through resonant electronic excitation of a polyanion.[17] The resultant PADs were shown to be dynamic, because the resonant alignment is lost as the initially created rotational wavepacket dephases with time. In this contribution we will also expand on these previously reported results, by considering in detail the shape of the RCB and we provide a reinterpretation of the temporal population dynamics following electronic excitation.

To investigate the effect of the RCB on the dynamics of PEs, we use doubly deprotonated pyrromethene-556 (PM^{2-}, Fig. 1). [24, 25] It is commonly used as a laser

dye and primarily consists of a central boron-dipyrromethene (BODIPY) chromophore, on which the highest occupied molecular orbital (HOMO) of the dianion is located, and two terminal SO_3^- groups carrying the excess charges. Numerous studies have investigated the BODIPY chromophore, which has a strong $S_1 \leftarrow S_0$ transition centered at 498 nm (in methanol) and a transition dipole moment vector as indicated in Fig. 1. [26-28] The electron affinity of PM^{2-} in the gas-phase has been measured as 1.6 eV, making the S_1 excited state formally unbound with respect to electron loss. [17] This state is however located below the RCB but above the D_0 monoanion ground state, such that the S_1 state is meta-stable. The choice of PM^{2-} is driven by a number of factors. Firstly, the optically bright S_1 state decays predominantly by fluorescence in solution ($\Phi = 0.92$ in methanol),[24, 29] such that internal conversion (IC) or inter-system crossing are very minor decay pathways in the condensed phase. The observed S_1 lifetime in the gas-phase is significantly faster[17] than the solution phase fluorescence lifetime (~5 ns in methanol[26, 29]), implying that fluorescence plays a negligible role in the decay of isolated excited PM^{2-}. Secondly, the rigid structural backbone of PM^{2-} does not change dramatically upon excitation. Hence, changes in the location of the charged sulfate groups relative to the BODIPY backbone can effectively be neglected. Thirdly, the location of the sulfate groups, and therefore the excess charges, is very well defined with respect to the transition dipole moment of the $S_1 \leftarrow S_0$ transition.

In this paper we present results of nanosecond and femtosecond single-color photoelectron (PE) imaging as well as pump-probe time-resolved PE imaging results and discuss in detail the observed PE spectra and anisotropy following resonant and non-resonant excitation

II. METHODS

5

A. EXPERIMENT

Isolated PM^{2-} was produced via an electrospray ionization source and investigated using femtosecond PE imaging. [30-32] The experimental setup has been described previously, and only details pertaining to the current experiment are given. [33, 34] Ions were produced via electrospraying of a 1 mM solution of the PM disodium salt (Exciton) in methanol at ~ −2.5 kV. Anions were introduced into vacuum by a desolvation capillary and accumulated in a home-built ring electrode ion trap. Stored ions were then ejected at 200 Hz into a collinear time-of-flight mass spectrometer. An ion packet of mass-selected PM^{2-} was intersected by laser pulses at the center of a velocity-map imaging arrangement[35] and PEs collected on a dual multi-channel plate detector with a phosphor anode. Raw PE images were captured with a CCD camera and deconvoluted using the polar onion-peeling (POP) algorithm developed in our group, [36] yielding PADs and PE spectra that have been calibrated using the well-known detachment from iodide. The energy resolution is ~5% of the *eKE*.

Nanosecond laser pulses in the visible spectral region were derived from an Nd:YAG pumped optical parametric oscillator. The nanosecond laser operated at 10 Hz and consequently the ions in these experiments were also injected into the mass-spectrometer at 10 Hz. Nanosecond pulse energies were attenuated to ~ 5 mJ per pulse. The intensity in the interaction region was on the order of 7×10^6 Wcm^{-2}.

Femtosecond laser pulses were derived from a commercial Ti:Sapphire oscillator and amplifier system delivering 800 nm, 35 fs pulses at 1 kHz repetition rate. Pulses at 266 nm were generated via frequency tripling using two type I beta-barium borate (BBO) crystals. Pulses across the visible were generated by mixing the output from a commercial optical parametric amplifier with remaining 800 nm fundamental light. Typical light intensities in the interaction region were on the order

of 1×10^{10} Wcm^{-2}, with a cross-correlations between 510 nm and the 800 nm fundamental of around ~ 130 fs, as determined in a separate thin BBO crystal.

B. THEORY

All electronic structure calculations were carried out using the Gaussian09 software package. [37] The structure of PM^{2-} was optimized at the B3LYP/6-311++g(2d,2p) level. The vertical detachment energy was evaluated as the difference in energy between the monoanion and dianion electronic configurations in the dianion optimized geometry. Electronic excited state calculations were carried out using time-dependent density functional theory (TD-DFT) at the B3LYP/6-311++g(2d,2p) level for both the monoanion and dianion of PM, in the optimized dianion geometry.

The RCB was calculated using the Local Static Approximation model developed by Dreuw and Cederbaum. [38] The dianion geometry was optimized using density functional theory at the B3LYP/6-311++g(2d,2p) level. RCB calculations were carried out with the 3-21+g* basis set for 2D scans and with the 6-311++g(2d,2p) basis set for 1D cuts through the potential energy surface. RCB energies were then evaluated as the difference in total energy between the monoanion electronic configuration in the dianion geometry, and the same configuration in the presence of a point charge. The location of the excess point charge (representing the departing PE) was scanned systematically to build up a 1D or 2D RCB surface. In order to avoid effects of the point charge on the molecular charge distribution (polarization effects), a small $-0.01e$ charge was used and the calculated energy differences scaled accordingly. [38]

III. RESULTS

A. SINGLE-COLOR PHOTOELECTRON SPECTRA

Single color PE spectra of PM^{2-} collected with a femtosecond laser pulse are shown in Fig. 2, along with the corresponding reconstructed photoelectron images (insets). The PE spectrum collected at a photon energy of 4.66 eV (266 nm) is shown in Fig. 2(a) and shows two distinctive features: a small broad peak centered at an electron kinetic energy (eKE) = 1.6 eV and a higher energy feature centered at eKE = 2.7 eV. The PADs are fitted to the well-known formula[39, 40]

$$I(\theta) = \frac{\sigma}{4\pi} \sum_{2n} \beta_n P_n(\cos\theta)$$

where σ is the photo-detachment cross section; $P_n(\cos\theta)$ and β_n are the nth order Legendre polynomial and anisotropy parameter, respectively; and n is an even integer corresponding to the number of photons absorbed in the detachment process. For one photon detachment, $n = 1$ so that only β_2 is required to fully describe the PADs (note that $\beta_0 = 1$). For a two-photon detachment, $n = 2$ and β_4 is additionally required to describe the PADs. The fitting is performed in the POP deconvolution routine.[36] The measured PE anisotropy parameter for the feature at eKE = 1.6 eV is $\beta_2 = 0.0 \pm 0.2$, while that at eKE = 2.7 eV has $\beta_2 = -0.12 \pm 0.05$.
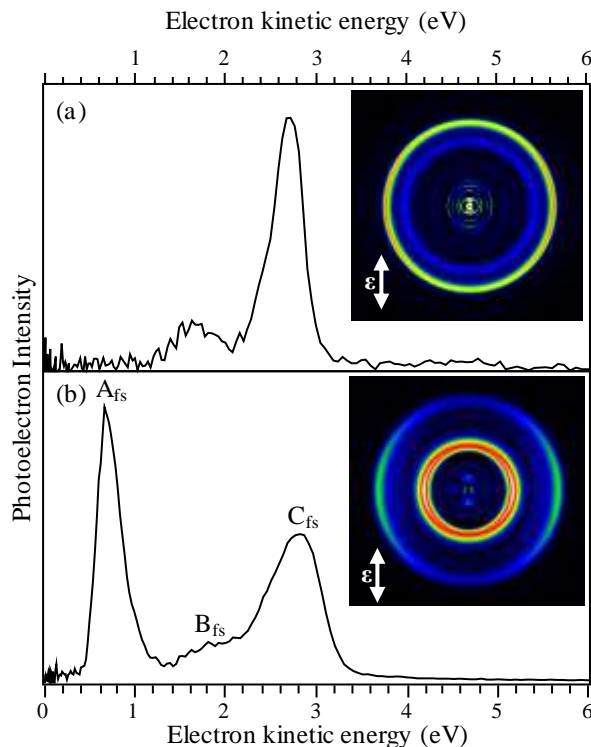
Figure 2: Photoelectron spectra of PM^{2-} taken at (a) 4.66 eV and (b) 2.43 eV. Insets show the respective reconstructed photoelectron images, in which ε indicates the polarization direction of the laser field. Adapted with permission from reference [17]. Copyright 2012 American Chemical Society.

The femtosecond PE spectrum collected at a photon energy of 2.43 eV (510 nm) is shown in Fig. 2(b). At this energy, the photon is resonant with the $S_1 \leftarrow S_0$ transition. Three distinct features are observed. Feature A_{fs} is a sharp and asymmetrically shaped peak centered around $eKE = 0.7$ eV, feature B_{fs} is weaker and centered at $eKE \sim 1.6$ eV, and feature C_{fs} is centered at $eKE = 2.8$ eV. Given that feature C_{fs} is at a higher eKE than the photon energy, this feature arises from a two-photon process. Further confirmation for this assignment can be gained from a comparison between the 4.66 eV and 2.43 eV PE spectra. The similarity in spectral shape and peak positions of features B_{fs} and C_{fs}, compared with the corresponding features in the UV PE spectrum, indicate that both features are arising from a 2-

9

photon process. The large feature in the 4.66 eV PE spectrum therefore comes from a single photon process. The intensity of the PE features in the 2.43 eV PE spectrum can be ascribed to the fact the 2-photon PE features (features B_{fs} and C_{fs}) are resonance enhanced by the $S_1 \leftarrow S_0$ transition. Feature A_{fs} in Fig. 2(b) is not reproduced in the 4.66 eV PE spectrum. The measured PE anisotropy parameters for features A_{fs}, B_{fs} and C_{fs} are: $\beta_2 = -0.15 \pm 0.08$; $\beta_2 = -0.6 \pm 0.1$; and $\beta_2 = -0.56 \pm 0.05$, respectively. The higher order parameters for B_{fs} and C_{fs} are $\beta_4 = 0.11 \pm 0.13$ and $\beta_4 = 0.02 \pm 0.05$, respectively, which are essentially zero within experimental error.

Femtosecond PE spectra collected at several photon energies resonant with the $S_1 \leftarrow S_0$ transition are shown in Fig. 3(a), with detachment energies ranging from 2.58 eV (479 nm) to 2.30 eV (539 nm). All spectra are similar in appearance to the PE spectrum taken at 2.43 eV with features A_{fs} and C_{fs} clearly distinguishable. The weaker feature B_{fs} is not as well reproduced because of the lower statistics in these spectra. As the photon energy increases, the intensity of feature C_{fs} increases relative to feature A_{fs}. Moreover, feature A_{fs} shows no spectral shift with increasing photon energy. This is in contrast to feature C_{fs}, which shifts to higher eKE as the photon energy increases, in agreement with the expected dependency of a vertical 2-photon photodetachment transition.

PE spectra of PM^{2-} collected with nanosecond laser pulses are shown in Fig. 3(b), for various photon energies ranging from 2.23 eV (540 nm) to 2.70 eV (460 nm). All spectra show three distinctive features. The first is an isotropic peak, feature D_{ns}, at very low eKE. A second broad feature centered at $eKE = 1.3$ eV is seen in the PE spectra taken at *all* detachment energies. This feature exhibits slightly negative anisotropies, with $\beta_2 = -0.17 \pm 0.09$ at 2.58 eV (480 nm). We label this feature A_{ns} for

10

reasons that will become apparent below. Finally, at higher *eKE* a broad feature between 2 and 3.5 eV can be discerned that shifts to higher *eKE* with increasing photon energy. This feature gains intensity relative to the other features as the photon energy is increased. Based on the *eKE* of this feature, it is safe to assign this feature to a resonance-enhanced 2-photon detachment process as discussed above for femtosecond excitation. Hence, we label this feature C_{ns}. It is significantly more anisotropic than feature A_{ns}, with typical values for $\beta_2 = -0.49 \pm 0.08$ ($\beta_4 = 0.02 \pm 0.12$) at 480 nm.
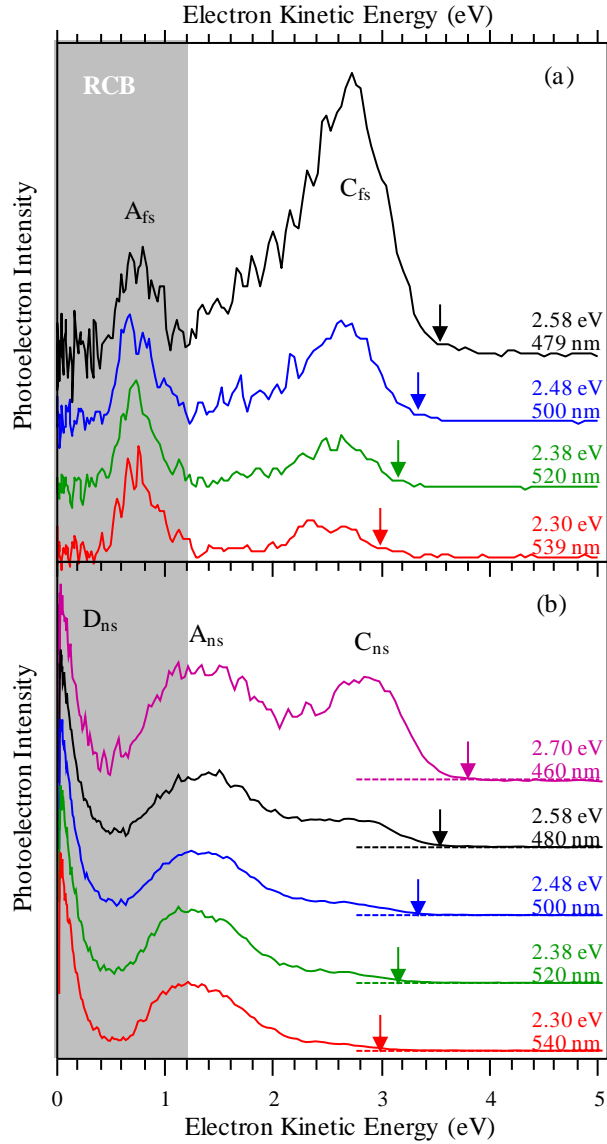
Figure 3: Photoelectron spectra of PM^{2-} taken with (a) femtosecond pulses and (b) nanosecond pulses over a range of photon energies as indicated. Downward vertical arrows show the maximum kinetic energy expected for a 2-photon transition at the given photon energy. The grey shading represents the spectral region where the RCB prevents direct electron detachment.

B. TIME-RESOLVED PHOTOELECTRON SPECTRA

Time-resolved dynamics of the S_1 dianion excited state were investigated at various pump energies (2.43, 2.34 and 2.30 eV, corresponding to wavelengths of 510, 530 and 539 nm, respectively) and probed at 1.55 eV (800 nm). Excitation at different pump energies leads to different amounts of internal energy within the S_1 excited state. Fig. 4(a) shows the PE spectrum when the pump and probe pulses are temporally overlapped, $t = t_0$. The probe alone produces no photoelectrons so that pump-probe spectra are directly comparable to the one-color (at 2.43 eV) PE spectrum in Fig. 2(b), where any new features must arise from a pump-probe process. A new PE feature is clearly observed between the pump-only features A_{fs} and C_{fs}. Two representative PE spectra taken at t_0 are shown in Fig. 4(a) for pump energies of 2.43 eV (510 nm) and 2.30 eV (539 nm). The two spectra show that the peak that can be assigned to feature A_{fs} does not shift with increasing pump photon energy. In contrast, a spectral blue shift is observed for the pump-probe feature as the photon energy is increased. Similarly, a blue shift in the resonance-enhanced 2-photon feature C_{fs} can be seen, which amounts to ~ 0.25 eV, consistent with a 2-photon process.

The dynamics were investigated by scanning the pump-probe delay, t, and integrating over the observed pump-probe PE feature as a function of t. The resulting dynamics traces are shown in Fig. 4(b) for the three pump photon energies used. The integrated PE intensities have been fitted with a single exponential decay, convoluted with a Gaussian instrument response function to account for the finite cross-correlation of pump and probe pulses. [41] This yields excited state lifetimes of 121, 112 and 117 ± 10 ps for pump wavelengths 510, 530 and 539 nm, respectively. All three lifetimes are identical within the error margins.
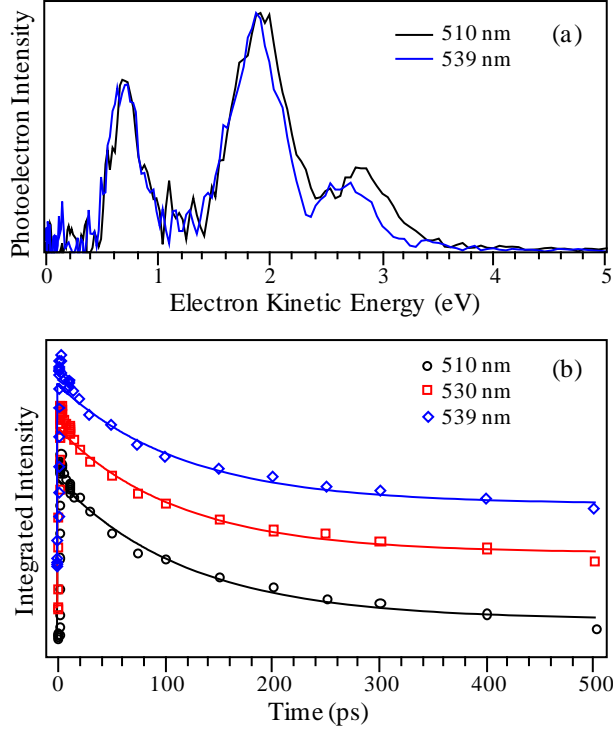
Figure 4: (a) Time-resolved photoelectron spectra of PM^{2-} at $t = t_0$ taken at two pump photon energies. (b) Integrated photoelectron signal of the pump-probe feature around $eKE \sim 2$ eV as a function of pump-probe delay at the photon energies indicated. Lines are fits to a single exponential decay.

IV. DISCUSSION

A. NON-RESONANT FEMTOSECOND PHOTOELECTRON SPECTRA

The high-energy peak in the 4.66 eV PE spectrum arises from single photon detachment, hence the photon energy must be greater than the adiabatic binding energy plus the repulsive Coulomb barrier (RCB). [10] In such a case, the asymptotic *eKE* can be related to the intrinsic energetics of the system in the usual fashion. Here the high energy peak is located at $eKE = 2.7$ eV, such that the vertical binding energy is 2.0 eV. Extrapolation of the high-energy side of this feature yields an adiabatic detachment energy that is approximately 1.6 eV.

14

To gain support for our assignment and to identify the final states accessed in the radical anion, we use DFT and TD-DFT calculations as described above. We calculate a vertical energy gap from the S_0 to the D_0 of 1.95 eV, while the adiabatic energy gap is evaluated to be 1.79 eV. This is in agreement with our measurements. The D_0 state corresponds to removal of an electron from the π-system of the BODIPY chromophore, and hence photodetachment from the S_0 is expected to lead to this electronic state of the anion.

Given the energy gap between the feature at eKE = 2.7 eV and the weaker peak at 1.6 eV, the latter most probably arises from the formation of an excited state in the radical anion following electron detachment. An excited state of the anion is calculated at 1.2 eV, corresponding primarily to excitation from the HOMO−3 to the HOMO of the anion. This state is weakly correlating with both the S_0 and S_1 state of the dianion, providing some support for this assignment.

For eKE < 1.1 eV, no PE signal is observed, despite the existence of several higher-lying D_n excited states of the monoanion that can be accessed according to our calculations. However, a low-energy cut-off in PE spectra of polyanions is expected because of the RCB, below which no PE can be emitted. Based on the 4.66 eV PE spectrum in Fig. 2(a), we estimate the RCB to be 1.1 eV high. This could indicate that a large fraction of the weak feature at eKE = 1.6 eV cannot be observed because of the proximity of the RCB. Based on the above considerations, we can construct an energy level diagram as shown in Fig. 5.
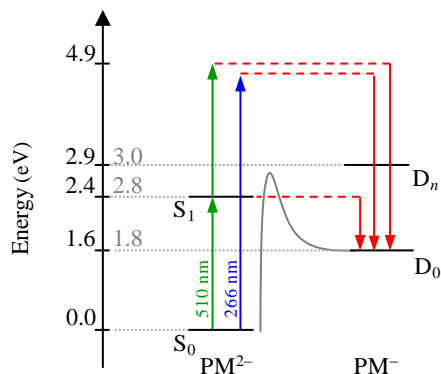
Figure 5: Energy level diagram of PM^{2-}. Black quantities indicate those determined by photoelectron spectroscopy, while grey quantities are those determined from DFT/TD-DFT calculations. Red downward arrows represent the kinetic energy of emitted photoelectrons.

While the RCB in dianions has been shown to strongly influence the direction of outgoing PEs, guiding them away from the remaining negative charges, [17, 19, 20] the observed PADs in the 4.66 eV PE spectrum are nearly isotropic. This implies that the differential photodetachment cross-section for PM^{2-} is almost isotropic, leading to an equal probability of detachment from any molecular orientation in space. Hence, there is no connection between the laboratory and molecular frame of reference, rendering the inherent molecular frame guiding of the PE by the RCB impossible to observe using this scheme. If instead the differential photodetachment cross-section is strongly peaking along a specific molecular orientation, [42] then the influence of the RCB on the outgoing PE can be observed as shown by the Wang group. [19, 20] However, with no prior knowledge of the detailed differential photodetachment cross-section, the degree of observed anisotropy is convoluted with this unknown and so can be difficult to interpret. To overcome this, the laboratory and molecular frames can be connected through molecular alignment, [43, 44] as discussed below.

16

B. RESONANT FEMTOSECOND PHOTOELECTRON SPECTRA AND ANGULAR DISTRIBUTIONS

The 2.43 eV PE spectrum shown in Fig. 2(b) shows some similarities with the PE spectrum at 4.66 eV. Features B_{fs} and C_{fs} are analogous to those observed following 1-photon detachment at 4.66 eV (Fig. 2(a)), but now proceed via the S_1 state in a resonance-enhanced 2-photon detachment scheme. However, in the 2.43 eV PE spectrum an additional feature (A_{fs}) can be seen at $eKE = 0.7$ eV, below the estimated 1.1 eV RCB height. In direct photodetachment, PE emission below the RCB is not possible. However, because the 2.43 eV photon is resonant with the $S_1 \leftarrow S_0$ transition, population will be transferred to the S_1 state of the dianion, where it is trapped by the potential barrier to photodetachment. Given that the S_1 state in PM^{2-} is a highly fluorescent state in solution,[26, 27, 29] it is not unreasonable to expect the lifetime of the S_1 state in the gas-phase to be sufficiently long to enable tunneling through the RCB, as has previously been observed in other dianion systems. [5, 21] We therefore assign feature A_{fs} to a tunneling process through the RCB from the S_1 excited state, leaving the anion in the D_0 ground state and producing a PE with eKE significantly below the height of the RCB. Note that such a process is allowed according to Koopmans' correlations in PM^{2-}. This tunneling feature is present at all employed wavelengths in Fig. 3(a), however no shift of the eKE with increasing photon energy is observed. This has previously been explained with a strongly adiabatic mechanism for tunneling through the RCB, which conserves excess internal energy during the tunneling process, leading to emission of electrons with constant eKE. [21] This is the situation encountered here and tunneling through the RCB is essentially a diagonal process.

All the resonant femtosecond PE spectra in Fig. 3(a) furthermore show a broad feature C_{fs} arising from a resonant 2-photon detachment process. The relative intensities of features A_{fs} and C_{fs} vary with increasing photon energy, with C_{fs} becoming more intense relative to A_{fs}. We can tentatively explain this by the presence of a higher-lying electronic state which can be accessed using two-photons. Evidence for this excited state can be seen in the solution phase absorption spectrum, which indicates that there is an absorption maximum at ~240 nm. [24, 27] Hence, as the photon energy is tuned to the blue, the second photon becomes more resonant with excitation of the S_1 to this higher lying state, increasing the detachment probability.

Comparison of the anisotropy of the features observed in the direct detachment at 4.66 eV with those observed following resonance-enhancement reveals significant differences. Both features B_{fs} and C_{fs} are observed to be strongly anisotropic following 2-photon detachment, and peaking in the direction perpendicular to the polarization vector of the laser, $\boldsymbol{\varepsilon}$, as indicated on the inset images in Fig. 2. This anisotropy can be traced to the influence of the RCB on the outgoing PE. [17] The probability of exciting the $S_1 \leftarrow S_0$ transition scales as a function of $\cos^2\theta$, where θ denotes the angle between the resonant electric field (laser polarization), $\boldsymbol{\varepsilon}$, and the direction of the transition dipole moment, $\mathbf{d_{01}}$. The $\mathbf{d_{01}}$ direction is shown in Fig. 1 and resonant excitation therefore leads to an ensemble of PM^{2-} molecules excited in their S_1 state that have their x-axis predominantly aligned with $\boldsymbol{\varepsilon}$. Absorption of a second photon then only probes the ensemble of S_1 excited molecules. As the laser field is only ~100 fs in duration, the S_1 excited PM^{2-} molecules are essentially frozen in space and the photoemission will occur from an *aligned* sample. Photodetachment from the S_1 state leads to the removal of an electron from the π system of the BODIPY chromophore and, according to our DFT

calculations, the resulting system with a hole on the BODIPY group and charged terminal sulfonates, is the lowest energy state, D_0. Given that there is a hole on the central chromophore and two negative charges on the SO_3 groups, one might intuitively expect the PE angular distribution to peak in the direction perpendicular to ε. This is what is observed and it is in stark contrast to the PE angular distribution of the similar feature in the single photon 4.66 eV PE spectrum, which is essentially isotropic. This clearly demonstrates the importance of establishing a connection between the laboratory and molecular frames of reference.

To gain additional insight into these qualitative arguments, a 2D cut through the RCB surface has been calculated. Shown in Fig. 6(a) is a contour map of the RCB in the *xy* plane of the molecule (where the Cartesian axes are shown in Fig. 1). Additionally, in Fig. 6(b) representative cuts through the RCB from the center of the molecule along each Cartesian coordinate are shown. As expected, the RCB is largest close to the terminal charges on the SO_3^- groups and falls off towards the center of the molecule. The maximum of the RCB is around 5 eV and it should be noted that free rotation around the C−S bond will smear out the local maxima identified at each O site. This explains why the cut along the *x*-axis is lower than this 5 eV RCB maximum. Along the *y*-axis, the RCB is asymmetric around the center of the molecule. A local maximum (3.2 eV) is observed near the electron rich boron center on the BODIPY chromophore. Along the positive *y*-direction, the lowest point in the RCB can be identified. The energy of this saddle point is 1.1 eV, in excellent agreement with the 4.66 eV PE spectrum *eKE* cut-off. It is furthermore consistent with the inability to directly detach an electron at 2.43 eV, given the adiabatic binding energy of 1.6 eV.
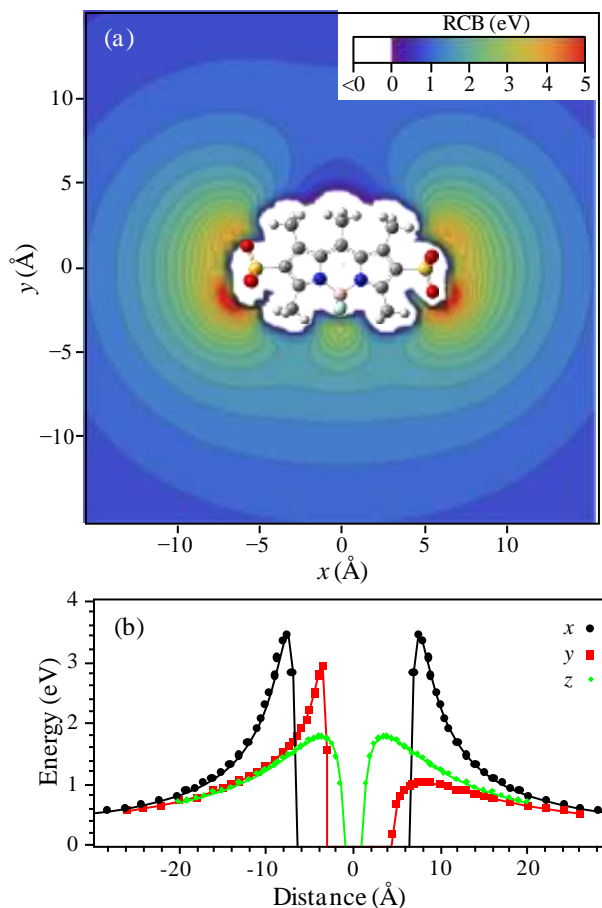
Figure 6: Calculated repulsive Coulomb barrier for PM$^-$ + e$^-$. (a) 2D RCB surface along the *x*-*y* plane (*z* = 0). (b) 1D cuts through the RCB originating at the center of the molecule, along representative Cartesian coordinates as defined in Fig. 1.

Following resonance-enhanced 2-photon detachment at 2.43 eV, the PE will have an asymptotic *eKE* of about 3.1 eV. Comparing this with the calculated RCB surface in Fig. 6(a) allows one to rationalize the observed PADs. The available kinetic energy is not sufficient for the electron to leave in the *x* direction (along the SO$_3^-$ groups), instead electrons will primarily be ejected along the +*y*-direction (or −*y*-direction as PM^{2-} is only 1D aligned). The lowest saddle point at 1.1 eV is quite shallow along the *x*-direction, suggesting that electrons could have quite a spread in angular emission. Hence we do not observe extreme anisotropy parameters of $\beta_2 = -1$,

The barrier indicated by the cut along the negative y-direction shows an RCB at the boron site of $\sim$ 3.2 eV, which is just above the electron energy of feature C_{fs} and so will inhibit detachment along this coordinate. However, either side of the boron, saddle-points in the RCB (at the electro-positive methyl groups) should enable the electron to escape through these gaps as the RCB height here is on the order of 2 eV.

Once the PE leaves the molecule it will experience a force due to the RCB, which will guide the electron. As this force is simply the gradient of the RCB, one might expect that the PE will be further guided to be perpendicular to the x-coordinate. Such an interpretation is based on classical arguments. Although this is clearly not appropriate to describe the photodetachment process, it does provide a very useful framework to qualitatively understand observations and the RCB guiding appears to overcome any inherent anisotropy resulting from the quantum mechanical interference of the outgoing partial waves. It would be of interest to investigate asymptotically the electron emission both using quantum and classical simulations, but this is beyond the scope of the present study. We note that, in principle, interference should be present in the angular coordinate as there is more than one path to reach a given point on the detector. We have made very careful and high-quality measurements in an attempt to observe such features, but were unsuccessful. One possible reason for this is the finite and relatively high temperature of the ions ($\sim$300 K).

No appreciable anisotropy is observed for the feature corresponding to tunneling through the RCB (feature A_{fs}), despite this process also relying on resonant excitation to the S_1 excited state. The key difference between this feature and features B_{fs} and C_{fs} is that tunneling is not a direct process and so the PE is not created "instantaneously" (*i.e.* within the laser field). Instead, PE emission occurs once the

excited state electron has had time to tunnel through the RCB. From the time-resolved PE dynamics shown in Fig. 4(b), this occurs on a timescale a few orders of magnitude longer than the rotational dynamics. In free space, PM^{2-} can rotate and the absence of anisotropy then suggests that the initially aligned ensemble of dianions in the S_1 excited state is no longer aligned in the laboratory frame due to rotational dephasing, resulting in an isotropic emission of electrons. The rotational dynamics can be tracked in real-time through the PAD of the pump-probe feature as we have recently shown. [17]

C. EXCITED STATE DYNAMICS

Following excitation to the S_1 state, the relaxation dynamics can be investigated using a delayed probe pulse. Representative PE spectra at $t = t_0$ are shown in Fig. 4(a). The pump-probe feature blue shifts with increasing photon energy, as expected for a direct (vertical) detachment process induced by the probe. As a function of time, no noticeable spectral changes are observed, except for a reduction in the intensity of the pump-probe feature. The time-varying intensity of this pump-probe feature is a direct reflection of the S_1 state population. However, the decay mechanism cannot be unambiguously determined. Given that a tunneling feature (A_{fs}) can be clearly identified, tunneling must be occurring. However, internal conversion and intersystem crossing are in principle also possible. Fluorescence will occur on a nanosecond timescale and may be expected to contribute in a very minor role given the ~120 ps lifetime. [26, 29] Intersystem crossing is improbable as BODIPY dyes in general are well-known for their very low rate of $S_1 \rightarrow T_1$ conversion. [24, 25] However, it cannot be conclusively ruled out. Finally, internal conversion is possible although it should be noted that the fluorescence quantum yield in solution is very high.

Some indication of the dominant pathway can be discerned by the dynamics of the tunneling feature A_{fs}. If tunneling was the only (or dominant) decay mechanism, one would expect to observe depletion in the intensity of feature A_{fs} at t_0, followed by a recovery that mirrors the decay dynamics of the pump-probe signal. [31, 45] If the dynamics were solely from tunneling, then the integrated PE counts of the depletion should equal that of the pump-probe feature, as observed in the fluorescein dianion. [21] This is not the case and feature A_{fs} shows no discernible depletion, although we note that the data for this is quite noisy. It therefore appears that the dominant decay mechanism is internal conversion (or intersystem crossing), rather than electron tunneling. This is surprising because of the dominant fluorescence decay path for PM in solution. The main difference between the isolated and solvated PM^{2-} is the stabilization of the SO_3^- groups. Minor environmental effects have been noted on PM in different solvents, but these have been associated with effects on the resonance structures of the BODIPY chromophore and the SO_3^- groups are essentially spectators. [29] Nonetheless, the fact that these groups are not solvated in the gas-phase leads to strong Coulomb interactions with the BODIPY chromophore π-system, which may open up internal conversion pathways from the S_1 excited state.

As the same pump-probe feature acts as a measure of both internal conversion and tunneling, the observed lifetime is a combination of the individual contributions ($k_{obs} = k_{IC} + k_{tunnel}$, where $k = \tau^{-1}$ is the rate constant). The measured ~120 ps is thus a lower bound of the internal conversion lifetime, while the tunneling kinetics will be significantly slower (*i.e.* $\tau_{tunnel} \gg 120$ ps).

D. EFFECT OF PULSE DURATION ON PHOTOELECTRON SPECTRA

The observed peak at very low eKE in the PE spectra taken with a nanosecond laser of Fig. 3(b), feature D_{ns}, is unexpected. As discussed before, the presence of the RCB should inhibit the emission of electrons at such low energy. This "forbidden" region is highlighted in Fig. 3 as a grey shaded area, extending to the lowest RCB height of 1.1 eV. Low energy features have been observed before by the Wang group in dicarboxylate dianions.[46] These were assigned to the dissociative autodetachment from an anion, formed following photodetachment of the parent dianion. Specifically, it was proposed that the parent radical anion can exothermically undergo decarboxylation forming the $(CH_2)_nCO_2^-$ radical, which can then undergo electron loss, leading to low energy PEs. Part of their assignment was based on the observed structure in the PE spectra at $eKE < 0.1$ eV. We also note that until the use of PE imaging to study the spectroscopy of polyanions (*i.e.* before 2008 [20]), such low eKE features would not have been observed because of the poor efficiency of magnetic bottle PE spectrometers at low eKE.

In the present case, the low energy electrons must also come from a mono-anion. However, the origin of the peak is rather different. This can be appreciated immediately by the fact that feature D_{ns} is not seen in the PE spectra taken with femtosecond pulses, even at very low intensities. Moreover, feature D_{ns} is structureless and isotropic, decaying exponentially with eKE. Exponentially decaying PE spectra peaking at threshold are often indicators for statistical autodetachment or thermionic emission. [47-50] Taking the above observations into account, and the fact that no fragmentation is expected following a single excitation to the S_1 state, we recognize that the system must be acquiring excessive amounts of internal energy, which can then lead to dissociation and electron loss.

The mechanism by which PM^{2-} can acquire such high internal energy (be it in electronic or vibrational degrees of freedom) can be reconciled by the fact that the nanosecond laser field remains resonant with the $S_1 \leftarrow S_0$ transition for the duration of the pulse width (~10 ns) and by the fact that the dominant decay pathway is internal conversion, which is occurring on a timescale that is at least one order of magnitude faster than the laser pulse. Thus many photons can be absorbed in a similar vein to IR multiphoton dissociation, but using an electronic rather than a vibronic transition. [51, 52] With each photon cycle, the internal energy is increased (by ~2.5 eV) and will ultimately lead to a sufficiently high internal energy that unimolecular decay will occur. Given the photon energy, this would require very few cycles. Our proposed picture is in agreement with the statistical nature (exponential decay and isotropy of the PAD) of feature D_{ns}.

The second feature in the nanosecond PE spectra (A_{ns}), centered at $eKE = 1.3$ eV, appears to show no shift towards higher eKE with increasing photon energy and may be correlated with feature A_{fs} in the femtosecond PE spectrum in Figs. 2(b) and 3(a). We have shown previously that the invariance of the peak eKE to detachment photon energy can be attributed to a strongly adiabatic electron tunneling process through the RCB. [21] This has a propensity to conserve the internal energy of the dianion into the anion as the electron is lost. The fact that features A_{fs} and A_{ns} do not shift with photon energy over a range of 0.4 eV indicates that a similar behavior may be responsible. However, some clear differences are also apparent between A_{fs} and A_{ns}.

The comparison between the tunneling peak in the femtosecond versus nanosecond experiments shows that the maxima of A_{fs} and A_{ns} are located at $eKE =$ 0.7 eV and 1.3 eV, respectively. Furthermore, the width has increased significantly in

A_{ns}. This is in contrast to our previous experiments on doubly-deprotonated fluorescein dianions, in which femtosecond and nanosecond spectra were identical. [21] The important difference between these two systems is that, in the fluorescein dianion, the tunneling lifetime is on the order of 1 ps, and therefore no photon cycling is possible. A similar observation has recently been reported in a tetra-anion. [22] When using femtosecond pulses, multiple photon cycling is also not possible, irrespective of tunneling life, and the PE spectra taken at different energies reveal no shift in feature A_{fs}, while feature C_{fs} clearly does shift (Fig. 3(a)).

The broadening observed in PM^{2-} is presumably a consequence of the internal heating induced by photon cycling. The lowest eKE of the tunneling feature is the same in both the femto- and nanosecond PE spectra and the broadening is only observed towards higher eKE. Moreover, the maximum of feature A_{ns} is at $eKE \sim 1.3$ eV, which is close to but just above the RCB height at 1.1 eV. This suggests that a significant fraction of the "tunneling" feature may contain contributions from detachment *above* the lowest RCB, enabled by the high internal energy. This would appear to contradict the strongly adiabatic tunneling picture observed in the fluorescein dianion. However, the timescales of the electron loss in the present case are much longer than in the fluorescein dianion. Complete intra-molecular vibrational redistribution (IVR) of the internal energy in PM^{2-} may be expected and so modes that lead to electron emission over the lowest barrier can be statistically sampled. Hence, non-adiabatic tunneling becomes possible and probably dominates in this long-time regime. Such a picture is consistent with both spectral broadening of feature A_{ns} relative to A_{fs} and a blue shift towards the lowest point of the RCB, which is close to the maximum observed in feature A_{ns}.
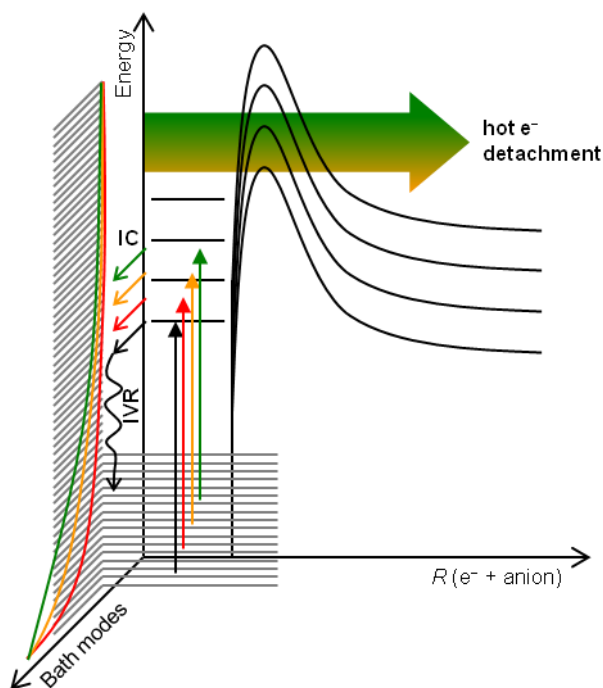
Figure 7: Schematic diagram explaining the photon-cycling scheme observed in PM^{2-} that ultimately leads to photoelectrons being emitted non-adiabatically just above the lowest RCB. Each color represents a successive cycle and the internal temperature (represented by population profiles of the bath modes) is shown to increase at every cycle by ~ 2.5 eV. After a small number of cycles, electrons can escape either from the S_1 excited state or the S_0 ground state, by accessing the continuum above the lowest RCB.

This mechanistic picture is outlined in Fig. 7. Upon excitation, the RCB experienced by the system increases because of the adiabatic tunneling, as discussed in the fluorescein dianion. The system undergoes IVR on the S_1 excited state. This is followed or in competition with internal conversion back to S_0, where additional IVR will occur. The system then absorbs additional photons, instigating the same cascading process. However, now there is already ~2.5 eV of internal energy in the system before photo excitation. Once in the S_1 with this additional internal energy content, IVR on the S_1 excited state could lead to a statistical sampling of the modes that lead to electron loss over the lowest RCB. Alternatively, this non-adiabatic tunneling process is also possible from the ground electronic state (S_0) following a small number of photon cycles. We have represented this latter scenario in Fig. 7, but experimentally, we cannot determine whether feature A_{ns} arises from non-adiabatic tunneling from the S_1 or S_0 states. Nevertheless, these statistical views are important

as it is through such mechanisms that electron loss and fragmentation can occur for thermally activated polyanions in tandem mass-spectrometry experiments. [53, 54]

In addition to this statistical emission over the RCB, tunneling may also contribute to the observed feature. The number and shape of RCB surfaces for both the S_1 and S_0 states will depend on the extent of internal excitation. Therefore, the relevant RCB surfaces after a photon cycle are likely to be different than those at 300 K. Hence, excitation from a hot S_0 ground state (after a photon cycle) will expose the S_1 state to different RCB surfaces and this may lead to broadening of the tunneling peak. This may be expected to be particularly important in non-rigid polyanions.

The PE feature attributed to resonance-enhanced 2-photon detachment with a nanosecond laser pulse (C_{ns}) exhibits strong anisotropies on the order of $\beta_2 = -0.5$ at all employed wavelengths. This is similar to those observed for feature C_{fs} following femtosecond excitation. In the latter case, the short pulse durations leads to the absorption of the second photon from an aligned ensemble, producing the highly anisotropic distribution of PEs. [17] This argument does not hold for nanosecond excitation as the second photon is likely to be absorbed significantly later than the typical rotational dephasing time (a few ps). One might therefore expect to observe an isotropic PE distribution.

A possible explanation for the observed anisotropy could be the involvement of a 2-photon resonance, discussed briefly above, due to the additional state seen at ~240 nm in the absorption spectrum. This resonance could lead to a non-isotropic absorption cross-section for the second photon, leading to a preferential resonance-enhanced process from a particular orientation and hence an anisotropic distribution of PEs. However, we have no experimental evidence to support this except for the relative increase in detachment of feature C_{fs} to A_{fs} seen in Fig. 3.

V. CONCLUSION

We have presented an extensive study of the gaseous dianion PM^{2-} using PE imaging with femtosecond and nanosecond laser pulses. The femtosecond measurements confirm the strongly adiabatic nature of electron tunneling through the RCB previously reported. However this was not the situation observed following nanosecond excitation, where the dominant internal conversion decay channel leads to multiple photon cycling via an electronic transition and the build-up of excessive amounts of internal energy in the system. Within the nanosecond pulse duration, this energy becomes redistributed and eventually samples modes leading to the detachment over the lowest RCB. This shifts the observed PE signal towards the lowest energy on the RCB surface. Hence the timescale of the excitation and available decay routes play a crucial role in interpreting PE spectra of dianions.

Using time-resolved photoelectron spectroscopy, the lifetime of the S_1 excited state was evaluated as ~120 ps, independent of excitation energy. The observed PE angular distributions can be rationalized with the molecular alignment following an allowed electronic transition. The direction of any outgoing PEs is strongly dependent on the RCB surface, an effect that outcompetes any inherent angular distribution due to partial wave interferences. The RCB was calculated using the Local Static Approximation approach and agrees qualitatively with experimental data.

VI. ACKNOWLDEGEMENTS

VII. REFERENCES

[1] A. Dreuw, and L. S. Cederbaum, Chem. Rev. **102**, 181 (2002).

[2] M. K. Scheller, R. N. Compton, and L. S. Cederbaum, Science **270**, 1160 (1995).

[3] X.-B. Wang, and L.-S. Wang, Annu. Rev. Phys. Chem. **60**, 105 (2009).

[4] O. T. Ehrler, J. M. Weber, F. Furche, and M. M. Kappes, Phys. Rev. Lett. **91**, 113006 (2003).

[5] O. T. Ehrler, J. P. Yang, A. B. Sugiharto, A. N. Unterreiner, and M. M. Kappes, J. Chem. Phys. **127**, 184301 (2007).

[6] K. Matheis, L. Joly, R. Antoine, F. Lepine, C. Bordas, O. T. Ehrler, A. R. Allouche, M. M. Kappes, and P. Dugourd, J. Am. Chem. Soc. **130**, 15903 (2008).

[7] J. Simons, J. Phys. Chem. A **112**, 6401 (2008).

[8] L. S. Wang, C. F. Ding, X. B. Wang, J. B. Nicholas, and B. Nicholas, Phys. Rev. Lett. **81**, 2667 (1998).

[9] X.-B. Wang, and L.-S. Wang, Nature **400**, 245 (1999).

[10] X. B. Wang, C. F. Ding, and L. S. Wang, Phys. Rev. Lett. **81**, 3351 (1998).

[11] R. N. Compton, A. A. Tuinman, C. E. Klots, M. R. Pederson, and D. C. Patton, Phys. Rev. Lett. **78**, 4367 (1997).

[12] R. L. Hettich, R. N. Compton, and R. H. Ritchie, Phys. Rev. Lett. **67**, 1242 (1991).

[13] C. Jin, R. L. Hettich, R. N. Compton, A. Tuinman, A. Derecskei-Kovacs, D. S. Marynick, and B. I. Dunlap, Phys. Rev. Lett. **73**, 2821 (1994).

[14] C. Yannouleas, and U. Landman, Chem,. Phys. Lett. **210**, 437 (1993).

[15]J. M. Weber, I. N. Ioffe, K. M. Berndt, D. Löffler, J. Friedrich, O. T. Ehrler, A. S. Danell, J. H. Parks, and M. M. Kappes, J. Am. Chem. Soc. **126**, 8585 (2004).

[16]X.-B. Wang, J. B. Nicholas, and L.-S. Wang, J. Chem. Phys **113**, 653 (2000).

[17]D. A. Horke, A. S. Chatterley, and J. R. R. Verlet, J. Phys. Chem. Lett. **3**, 834 (2012).

[18]C.-G. Ning, P. D. Dau, and L.-S. Wang, Phys. Rev. Lett. **105**, 263001 (2010).

[19]X.-P. Xing, X.-B. Wang, and L.-S. Wang, J. Phys. Chem. A **113**, 945 (2008).

[20]X. P. Xing, X. B. Wang, and L. S. Wang, Phys. Rev. Lett. **101**, 083003 (2008).

[21]D. A. Horke, A. S. Chatterley, and J. R. R. Verlet, Phys. Rev. Let. **108**, 083003 (2012).

[22]H.-T. Liu, J.-P. Yang, M.-O. Winghart, T. J. A. Wolf, A.-N. Unterreiner, P. Weis, Y.-R. Miao, C.-G. Ning, M. M. Kappes, and L.-S. Wang, Phys. Rev. A **85**, 064503 (2012).

[23]M.-O. Winghart, J.-P. Yang, M. Kuhn, A.-N. Unterreiner, T. J. A. Wolf, P. D. Dau, H.-T. Liu, D.-L. Huang, W. Klopper, L.-S. Wang, and M. M. Kappes, Physical Chemistry Chemical Physics **15**, 6726 (2013).

[24]S. C. Guggenheimer, J. H. Boyer, K. Thangaraj, M. Shah, M.-L. Soong, and T. G. Paviopoulos, Appl. Opt. **32**, 3942 (1993).

[25]T. G. Pavlopoulos, M. Shah, and J. H. Boyer, Opt. Commun. **70**, 425 (1989).

[26]Y. Assor, Z. Burshtein, and S. Rosenwaks, Appl. Opt. **37**, 4914 (1998).

[27]F. López Arbeloa, J. Bañuelos, V. Martînez, T. Arbeloa, and I. López Arbeloa, Int. Rev. Phys. Chem. **24**, 339 (2005).

[28]A. Loudet, and K. Burgess, Chem. Rev. **107**, 4891 (2007).

[29]T. López Arbeloa, F. López Arbeloa, and I. López Arbeloa, Phys. Chem. Chem. Phys. **1**, 791 (1999).

[30]R. Mabbs, E. R. Grumbling, K. Pichugin, and A. Sanov, Chem. Soc. Rev. **38**, 2169 (2009).

[31]J. R. R. Verlet, Chem. Soc. Rev. **37**, 505 (2008).

[32]G. Wu, P. Hockett, and A. Stolow, Phys. Chem. Chem. Phys. **13**, 18447 (2011).

[33]J. Lecointre, G. M. Roberts, D. A. Horke, and J. R. R. Verlet, J. Phys. Chem. A **114**, 11216 (2010).

[34]D. A. Horke, G. M. Roberts, J. Lecointre, and J. R. R. Verlet, Rev. Sci. Instr. **83**, 063101 (2012).

[35]A. T. J. B. Eppink, and D. H. Parker, Rev. Sci. Instr. **68**, 3477 (1997).

[36]G. M. Roberts, J. L. Nixon, J. Lecointre, E. Wrede, and J. R. R. Verlet, Rev. Sci. Instr. **80**, 2009).

[37]M. J. Frisch, G. W. Trucks, H. B. Schlegel, G. E. Scuseria, M. A. Robb, J. R. Cheeseman, G. Scalmani, V. Barone, B. Mennucci, G. A. Petersson, H. Nakatsuji, M. Caricato, X. Li, H. P. Hratchian, A. F. Izmaylov, J. Bloino, G. Zheng, J. L. Sonnenberg, M. Hada, M. Ehara, K. Toyota, R. Fukuda, J. Hasegawa, M. Ishida, T. Nakajima, Y. Honda, O. Kitao, H. Nakai, T. Vreven, J. J. A. Montgomery, J. E. Peralta, F. Ogliaro, M. Bearpark, J. J. Heyd, E. Brothers, K. N. Kudin, V. N. Staroverov, R. Kobayashi, J. Normand, K. Raghavachari, A. Rendell, J. C. Burant, S. S. Iyengar, J. Tomasi, M. Cossi, N. Rega, J. M. Millam, M. Klene, J. E. Knox, J. B. Cross, V. Bakken, C. Adamo, J. Jaramillo, R. Gomperts, R. E. Stratmann, O. Yazyev, A. J. Austin, R. Cammi, C. Pomelli, J. W. Ochterski, R. L. Martin, K. Morokuma, V. G. Zakrzewski, G. A. Voth, P. Salvador, J. J. Dannenberg, S. Dapprich, A. D. Daniels, ñ. Farkas, J. B. Foresman, J. V. Ortiz, J. Cioslowski, and D. J. Fox, 2009).

[38]A. Dreuw, and L. S. Cederbaum, Phys. Rev. A **63**, 049904 (2001).

[39]J. Cooper, and R. N. Zare, J. Chem. Phys. **48**, 942 (1968).

[40]K. L. Reid, Annu. Rev. Phys. Chem. **54**, 397 (2003).

[41]D. A. Horke, and J. R. R. Verlet, Phys. Chem. Chem. Phys. **13**, 19546 (2011).

[42]D. Dill, J. Chem. Phys. **65**, 1130 (1976).

[43]K. F. Lee, D. M. Villeneuve, P. B. Corkum, A. Stolow, and J. G. Underwood, Phys. Rev. Lett. **97**, 173001 (2006).

[44]H. Stapelfeldt, and T. Seideman, Rev. Mod. Phys. **75**, 543 (2003).

[45]G. M. Roberts, J. Lecointre, D. A. Horke, and J. R. R. Verlet, Phys. Chem. Chem. Phys. **12**, 6226 (2010).

[46]X.-P. Xing, X.-B. Wang, and L.-S. Wang, J. Phys. Chem. A **114**, 4524 (2010).

[47]B. Baguenard, J. C. Pinaré, C. Bordas, and M. Broyer, Phys. Rev. A **63**, 023204 (2001).

[48]B. Baguenard, J. C. Pinaré, F. Lépine, C. Bordas, and M. Broyer, Chem. Phys. Lett. **352**, 147 (2002).

[49]K. Hansen, K. Hoffmann, and E. E. B. Campbell, J. Chem. Phys. **119**, 2513 (2003).

[50]M. Kjellberg, O. Johansson, F. Jonsson, A. V. Bulgakov, C. Bordas, E. E. B. Campbell, and K. Hansen, Phys. Rev. A **81**, 023202 (2010).

[51]N. Basov, E. Markin, A. Oraveski, A. Pankrato, and A. Skachkov, JETP Lett. **14**, 165 (1971).

[52]D. P. Little, J. P. Speir, M. W. Senko, P. B. O'Connor, and F. W. McLafferty, Anal. Chem. **66**, 2809 (1994).

[53]S. Ard, N. Mirsaleh-Kohan, J. D. Steill, J. Oomens, S. B. Nielsen, and R. N. Compton, J. Chem. Phys. **132**, 094301 (2010).

[54]H. J. Cooper, K. Hakansson, and A. G. Marshall, Mass Spectrom. Rev. **24**, 201 (2005).